ELSEVIER

Ceramics International 31 (2005) 973–980

CERAMICS INTERNATIONAL

www.elsevier.com/locate/ceramint

Colloidal processing, sintering and static grain growth behaviour of alumina-doped cubic zirconia

S. Tekeli*, U. Demir

Materials Division, Metallurgy Education Department, Faculty of Technical Education, Gazi University, 06500 Besevler-Ankara, Turkey

Received 22 July 2004; received in revised form 25 August 2004; accepted 1 October 2004
Available online 12 January 2005

Abstract

In order to determine the influence of alumina content on sintering and static grain growth behaviour of cubic zirconia, high purity commercial powders of 8 mol% yttria-stabilized cubic zirconia (8YSCZ) doped with 0, 1, 5, 10 wt.% Al_2O_3 were used. Colloidal processing was used for the mixing of powders in order to achieve a uniform distribution and homogeneous microstructure. The specimens were sintered at different temperatures between 1250 and 1400 °C for 1 h. The density increased with Al_2O_3 content up to 0.5 wt.% and a further increase in Al_2O_3 content led to a decrease in density. The enhanced density with increasing Al_2O_3 content up to 0.5 wt.% could be due to the rearrangement of Al_2O_3 particles during the early stages of sintering. The decreased density and grain growth in higher amount of Al_2O_3-doped specimens were due to the lower grain boundary diffusivity and mobility. X-ray diffraction results showed that Al_2O_3 had very limited solubility of 0.3 wt.% into 8YSCZ. The grain growth in the 0–10 wt.% Al_2O_3-doped 8YSCZ was studied. The experimental results showed that the grain growth in Al_2O_3-doped 8YSCZ occurred slowly and was more sluggish than that in undoped 8YSCZ. Also, the grain growth rate decreased with increasing Al_2O_3 content. The static grain growth exponent value and the activation energy for undoped 8YSCZ were found to be 2 and 289 kJ/mol, respectively. The addition of Al_2O_3 raised the grain growth exponent value to 3 and activation energy for the grain growth process was increased from 289 to 410 kJ/mol.

Keywords: A. Grain growth; Cubic zirconia; Sinterability; Alumina and colloidal processing

1. Introduction

Pure zirconia exists in three different crystal structures, i.e. monoclinic, tetragonal and cubic. These phases can be obtained depending on temperature and compositional ranges under equilibrium conditions. Monoclinic zirconia is present below 1240 °C and is the stable room temperature phase of pure zirconia. Tetragonal zirconia is an intermediate phase, which exists between 1240 and 2370 °C. The retention of the tetragonal phase can be controlled by the formation of a solid solution with alloying oxides such as MgO, CaO, Y_2O_3 and CeO_2. Cubic zirconia is the highest temperature phase, which is present in the temperature range of 2370 and 2680 °C [1–4]. However, upon the addition of a few percent of above oxides, the cubic phase can be obtained at lower temperatures [2,3]. The high temperature cubic phase can also be retained at room temperatures as a non-equilibrium phase by rapid cooling such that diffusive transformation does not occur.

Among zirconia phases, yttria-stabilized cubic zirconia (YSCZ) with fluorite structure is well-known as a solid electrolyte that possesses high oxygen ionic conductivity and chemical stability over wide ranges of temperature and oxygen partial pressure and thus it is widely used as an oxygen sensor, thermal barrier and solid oxide fuel cell (SOFC) electrolyte [5]. In SOFC applications, not only high ionic conductivity, but also better mechanical, chemical and electrical stability are required at high working temperatures (∼1000 °C is usually needed for SOFC and such a high working temperature leads to a lower working efficiency). Also low mechanical strength of cubic zirconia at higher and

* Corresponding author. Tel.: +90 312 4399760; fax: +90 312 2120059.
E-mail address: stekeli@gazi.edu.tr (S. Tekeli).

0272-8842/$30.00
doi:10.1016/j.ceramint.2004.10.011

longer working temperatures would limit their use as electrolytes, because they may fracture due to thermal stresses and mechanical stresses during operation, lack of transformation toughening and severe grain growth [6]. It is known that cubic zirconia has a large grain size and high grain growth rates [7]. Therefore, the enhancement of mechanical properties of the solid electrolyte is an important problem to be solved. Many approaches have been made to enhance the mechanical strength and hinder the severe grain growth in cubic zirconia [8]. One such approach is to use additives for the preventation of grain growth and thus the enhancement of mechanical properties.

The objective of the present study is to investigate the effect of Al_2O_3 addition between 0 and 10 wt.% on the sintering and static grain growth behaviour of 8 mol% yttria-stabilized cubic zirconia.

2. Materials and procedures

The materials used in the present work were 8 mol% yttria-stabilized cubic zirconia (8YSCZ) powder and high purity (>99.999%) alumina powder (α-Al_2O_3), supplied by Mandoval Ltd. Zirconia Sales (U.K.) Ltd. The average particle sizes were 0.3 μm for 8YSCZ and 0.4 μm for α-Al_2O_3. The chemical composition of the powders is listed in Table 1.

A colloidal processing route was used for the preparation of specimens for density, grain growth, phase content and lattice parameter measurements. Colloidal processing allowed homogeneous dispersion of powders and the economical production of net shapes. The slurry was prepared by dispersing the designated amounts of the powders (8YSCZ and α-Al_2O_3) in distilled water with a dispersing agent (Dispex A40); the slurry was then ball-milled for 24 h to obtain a good dispersion and to break-up agglomerates in a plastic container using zirconia balls. The milled slurry was injected by a syringe into a plaster mould. Cast specimens were released from the mould after ~60 min and then air-dried at ~25 °C for a few days. The green density of slurry-cast specimens was between 45 and 55% of the theoretical density. These specimens were presintered at 950 °C to make them more easy to be handled and smooth surfaces were obtained by carefully grinding off any casting protrusions. For the determination of the effect of shaping process on sintering, a batch of specimens of undoped 8YSCZ were also prepared by die-pressing which was carried out in a steel die at a pressure of 40 MPa.

For density, grain growth, phase analysis and lattice parameter measurements, 8YSCZ specimens containing Al_2O_3 dopant in amounts up to 10 wt.% were used. The green density of the slurry-cast and die-pressed specimens was measured from the volume and weight.

To determine optimal sintering temperature, the specimens were sintered at different temperatures between 1250 and 1400 °C in air at a constant heating rate of 200 °C/h. for 1 h. The density of sintered specimens was determined by the Archimedes method. The theoretical densities of the composites alumina and cubic–zirconia were estimated by the rule of mixtures, using 3.99 and 5.95 g/cm^3, respectively. The relative density was estimated on the assumption that the sintered body was of the cubic phase and based on the theoretical density of 5.92, 5.81 and 5.67 for the specimens doped with 1, 5 and 10 wt.% α-Al_2O_3, respectively.

The specimens for grain growth measurements were first sintered at 1400 °C for 1 h before annealing. Static grain growth was examined by annealing the sintered specimens for 10, 50 and 100 h at temperatures between 1400 and 1600 °C. After annealing, the specimens were sectioned, ground, polished to 1 μm surface-finish and finally thermally etched in air for 30 min at a temperature 50 °C lower than annealing temperature. Scanning electron microscopy (SEM) equipped with an energy dispersive X-ray spectrometer (EDS) attachment was used to characterize the microstructure of as-sintered and annealed specimens. Grain sizes were measured by the mean linear intercept method. An average grain size was obtained by multiplying 1.78 to average intercept lengths over 1000 grains. Phase content and lattice parameters were determined using XRD with Cu Kα radiation. A scan speed of 0.1 2θ/min was employed in the 20–60° 2θ range.

3. Results and discussion

Colloidal processing offers many possibilities and advantages over some other methods. First, a wide variety of particle size distributions can be slurry-cast into test specimens. Second, tooling is relatively inexpensive, often costing much less than equivalent injection moulding tooling. Third, the process is more readily adaptable to larger shapes. Finally, it is possible to produce near-net shape parts [9]. A major problem in the processing of nano-sized powders is existence of agglomerates, which occur spontaneously due to van der Waals forces. While small interparticle pores are easily closed during sintering, large

Table 1
Chemical composition of the powders

Materials	Composition (wt.%)							
	ZrO_2 (+HfO_2)	Y_2O_3	Al_2O_3	SiO_2	TiO_2	Fe_2O_3	Na_2O	CaO
8YSCZ	85.9	13.6	0.25	0.1	0.10	0.003	0.01	0.02
α-Al_2O_3	–	–	99.9	0.04–0.08	–	0.01–0.02	0.08	–

interagglomerate pores need a high sintering temperature or long sintering times to be eliminated. Pores exceeding a critical size even grow during sintering. Hence, significant grain growth takes place. To achieve better mechanical behaviour, fine grain size, homogeneous microstructure and high density are necessary. Colloidal processing helps to prevent the agglomeration of fine particles and allows the particle dispersion to be controlled during powder processing. In the present study, the agglomerates which often shrink away from the surrounding powder matrix during sintering causing crack-like voids, responsible for early fracture and leaving big pores in the microstructure after sintering were eliminated by colloidal processing. To demonstrate this, two sets of specimen were prepared by the production processes of die-pressing and slurry casting from undoped 8YSCZ. For the die-pressing tests, the powder was die-pressed into pellets under a compaction pressure of 40 MPa. The same size pellets were slurry-cast for comparison. The specimens obtained by these processes were then sintered at a heating rate of 200 °C/h. Fig. 1 shows the sintering curves of undoped 8YSCZ, prepared by two shaping processes. The specimens processed by slurry casting had a faster sintering rate and lower temperatures and the optimum sintering temperature was lower than that of the die-pressed one. In particular, the former achieved a density of 99% of its theoretical value at 1400 °C, while the latter reached the same value at 1450 °C. The reason for this enhancement was due to the homogeneous dispersion of powder and elimination of agglomerates in slurry-cast specimens, compared to die-pressed specimen in which agglomeration caused non-homogeneous sintering, leaving crack-like voids responsible for early fracture. Also, the die-pressing yields less efficient packing of the powders and larger pores than slurry casting; these features are known to retard effective sintering.

By XRD analysis, only cubic phase was detected and there were no diffraction peaks of second phases for all compositions. Fig. 2 shows the variation of the average lattice parameter of the cubic lattice with Al_2O_3 dopant content. As can be seen from this figure, the average lattice parameter of 8YSCZ linearly decreased with increasing Al_2O_3 content up to 0.3 wt.% and the parameter did not vary with further increase in the Al_2O_3 content. The linearity, which corresponds to Vegard's law, shows that solid solubility limit of Al_2O_3 in 8YSCZ is about 0.3 wt.%. The lower values of the lattice parameter found for Al_2O_3-doped 8YSCZ could be due to the substitution of smaller Al^{3+} ions for Zr^{4+} and Y^{3+} ions in the cubic lattice. The ionic radii of Al^{3+}, Y^{3+} and Zr^{4+} for eight-fold coordination are 0.52, 1.015 and 0.84 Å, respectively. As the solubility limit of Al_2O_3 in 8YSCZ is ~0.3 wt.%, Al_2O_3 can hardly form a solid solution with 8YSCZ. Therefore, Al_2O_3 mostly segregates around the 8YSCZ particles and at grain boundaries. There are two factors, which may contribute to the segregation of ions at the grain boundaries of oxide ceramics [10,11]. One is the strain energy relaxation that results from the size mismatch between the solute and host ions, and the other is electrostatic charge compensation. The size mismatch can be approximated in terms of misfit value Σ as follows:

$$\Sigma = \frac{r_1 - r_2}{r_1} \quad (1)$$

where r_1 and r_2 are the ionic radii of solvent and solute ions. The strain energy relaxation is the principal driving force for the segregation, when the misfit value is large. It is found that the misfit value of Al^{3+} is 0.36, and a large driving force

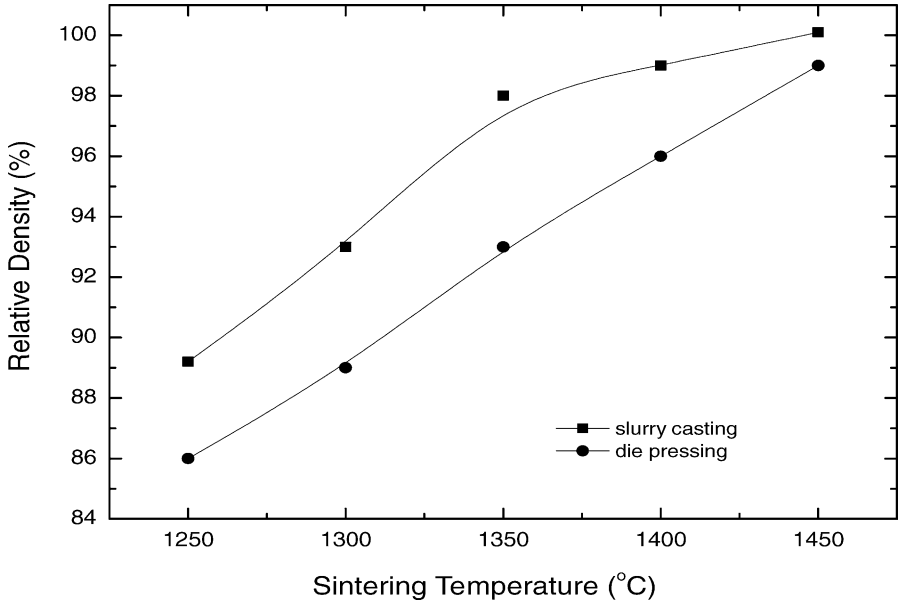

Fig. 1. Sintering curves of undoped 8YSCZ specimens prepared by slurry casting and die-pressing.

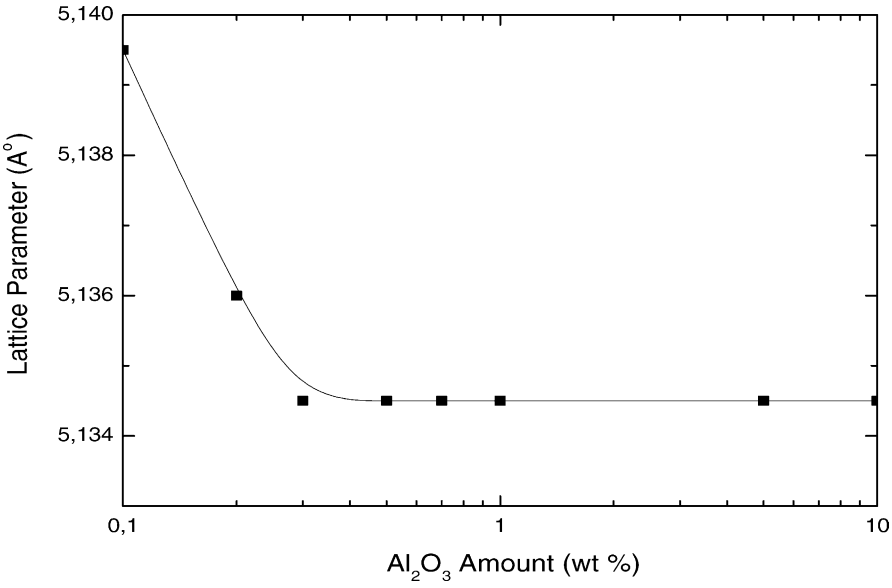

Fig. 2. Variation of lattice parameter with Al_2O_3 content.

for segregation at grain boundaries, instead of forming solid solution in matrix, is expected for trivalent Al^{3+} because of the considerable size mismatch and the charge difference between Al^{3+} and Zr^{4+}.

Fig. 3 shows the effect of sintering temperature and the Al_2O_3 content on the densification of 8YSCZ. For all compositions, the relative density of the specimens increased with elevating sintering temperature. It can be seen from this figure that a small amount of Al_2O_3 doping slightly increased the density. For all compositions between 0.3 and 0.5 wt.%, Al_2O_3-doped specimens provided the maximum sintered densities. This enhanced density with increasing Al_2O_3 content could be due to the rearrangement of Al_2O_3 particles during the early stages of sintering. However, further increase in Al_2O_3 content led to a decrease in sintered density. Higher sintering temperatures were necessary to densify the specimens containing higher Al_2O_3 contents, compared with the specimens with lower amounts of Al_2O_3. The retardation of densification in specimens with higher amount of Al_2O_3 particles in 8YSCZ could be due to a number of reasons. First, the microstructural investigations showed that the specimens with up to 1 wt.% Al_2O_3 addition were very dense and free from porosities in the grain interiors. This suggests that the small amount of Al_2O_3 addition located at the grain boundaries of 8YSCZ was sufficient for improving the densification. However, in specimens with higher amount of Al_2O_3 additions, there were many porosities in the grain interior and along the grain boundaries. These porosities hindered the sintered density and grain growth. Second, the distribution of Al_2O_3 grains in

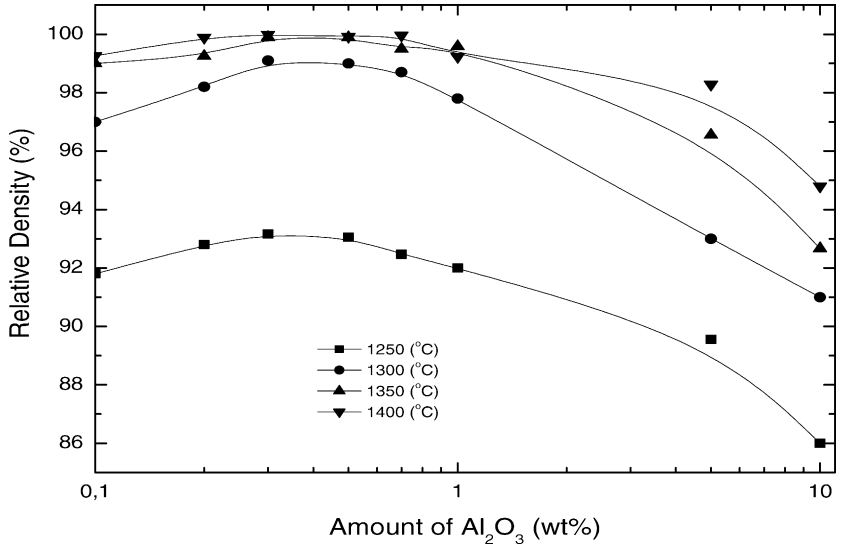

Fig. 3. The effect of sintering temperature and the Al_2O_3 content on the densification of 8YSCZ.

8YSCZ matrix was extremely difficult (although the colloidal processing was used to disperse the powders homogeneously) which could probably decrease the sintering rate by inducing tensile mean stress developed by differential shrinkage characteristics between 8YSCZ and Al_2O_3 grains. Finally, grain boundary diffusivity of 8YSCZ could be decreased by the Al_2O_3 addition, because the zirconia grains around the perimeter of the Al_2O_3 particles were unable to contact each other freely. As known, the grain boundary diffusion is the predominant mechanism of matter transport. Al_2O_3 grains mostly located at and around grain boundaries, which caused grain boundary diffusion path longer and thus the diffusion of atoms along grain boundaries between 8YSCZ and Al_2O_3 became slower. These results indicated that, higher amount of Al_2O_3 addition inhibited densification and grain growth by decreasing grain boundary diffusivity and mobility.

Static grain growth was examined by annealing fully dense sintered samples for various times between 10 and 100 h and at temperatures between 1400 and 1600 °C. Representative microstructures of undoped and various amount of Al_2O_3-doped 8YSCZ specimens annealed at 1500 °C for 10 h in air are shown in Fig. 4. The comparison of the grain size of the alloys at the same heat-treatment indicated that grains were larger in undoped 8YSCZ than in Al_2O_3-doped 8YSCZs. Also, the grain size decreased with increasing Al_2O_3 content. As shown in Fig. 4, Al_2O_3 particles can be seen for specimens with Al_2O_3 content >5 wt.%. This suggests that only a small part of Al_2O_3 dissolved in 8YSCZ and the rest of Al_2O_3 segregated at grain boundaries of 8YSCZ.

The static grain growth can be determined using the following phenomenological equation:

$$D^n - D_o^n = k(t - t_o) \tag{2}$$

$$k = k_o \exp\left(\frac{-Q}{RT}\right) \tag{3}$$

where, D is the grain size at time t, D_o is the reference grain size at time t_o, n is a constant for a given grain growth mechanism, k is a temperature-dependent constant, k_o is a temperature insensitive constant and Q, R and T are activation energy, gas constant and absolute temperature, respectively. The grain growth exponent can have a value between 1 and 4 depending on the rate-limiting step during grain boundary migration. The grain growth exponent, n, is calculated from the slope of the log (grain size) versus log (-time) line plot, which is equal to $1/n$. An example of such a plot is given in Fig. 5 for annealing at 1400 °C. It is evident that grains became larger during high temperature annealing and the extent of grain growth increased with increase in annealing temperature, time and with decrease in Al_2O_3 content. Also it can be seen from Fig. 5 that grain growth rates could be controlled by the deliberate addition of grain boundary phase of Al_2O_3. The grain growth exponent value of 2 for undoped 8YSCZ was obtained. However, with the

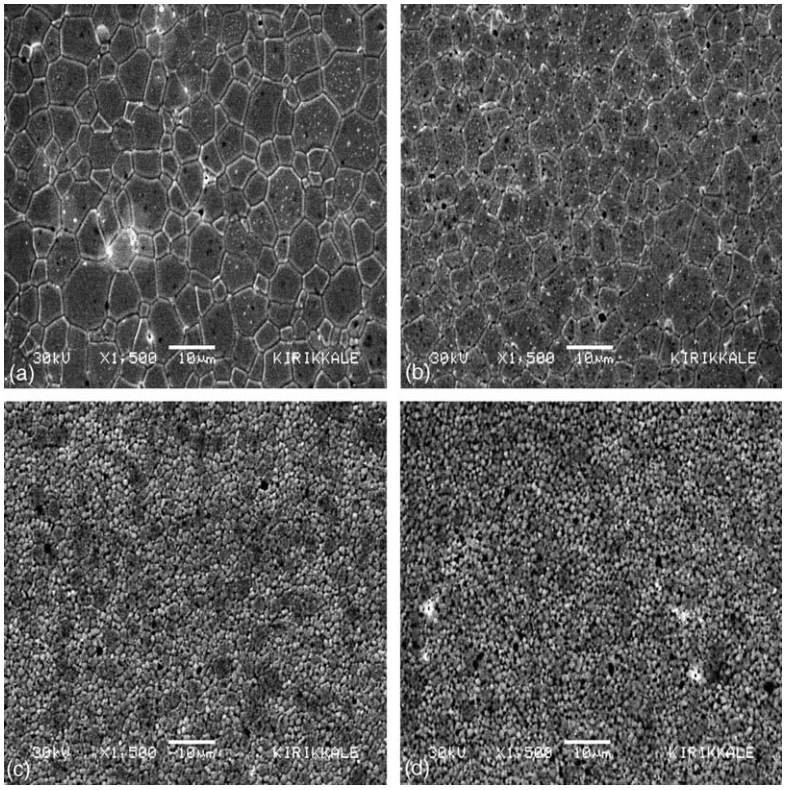

Fig. 4. SEM micrographs of 8YSCZ specimens annealed at 1500 °C for 10 h, containing: (a) 0 wt.% Al_2O_3; (b) 1 wt.% Al_2O_3; (c) 5 wt.% Al_2O_3; and (d) 10 wt.% Al_2O_3.

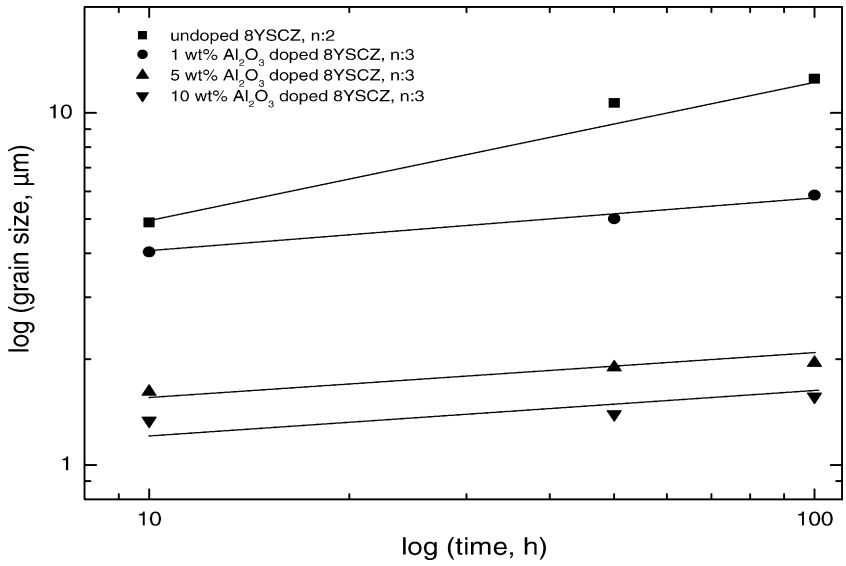

Fig. 5. Log (grain size) vs. log (time) for annealing at 1400 °C.

addition of Al_2O_3 up to 10 wt.%, the n value was increased to 3. In the case of single-phase growth, the exponent n usually takes a value of 2, which shows normal grain growth. In a dual phase structure, the steady state grain growth would occur such that the growth of one phase is affected by other phase grains, i.e. the grain growth is mutually restricted by Zener's pinning because of minor phase grains, as in metallic materials and that the coarsening of the minor phase is approximated by Ostwald ripening, then $n = 3$ can be predicted for lattice-diffusion controlled grain growth [12].

The activation energy for grain growth is calculated from the slope of log $((D^n - D_o{}^n)/t)$ versus $1/T$ as shown in Fig. 6. It can be seen from this figure that, the activation energy, Q, for Al_2O_3-doped 8YSCZs is higher than that for undoped 8YSCZ. The activation energy of undoped 8YSCZ was calculated as 289 kJ/mol. However, the addition of Al_2O_3 resulted in a gradual increase in activation energy. The activation values obtained are 361 kJ/mol for 1 wt.% Al_2O_3-doped 8YSCZ, 391 kJ/mol for 5 wt.% Al_2O_3-doped 8YSCZ and 410 kJ/mol for 10 wt.% Al_2O_3-doped 8YSCZ. This increase in activation energy is accompanied by a decrease in grain size. In order to reduce or suppress the grain growth, the grain boundary mobility and energy can be reduced, for example by impurities, pores, dopants or particles of a second phase. In polycrystalline materials, it has been shown that particles of a second phase with limited solubility are especially effective in pinning grain boundaries and thus in minimizing static and dynamic grain growth [13]. As stated by Sturm et al. [14], in order to provide efficient grain boundary pinning in a nanocrystalline structure, the particles of the second phase have to fulfil several of the following conditions; (a) small diffusion coefficient of the solute

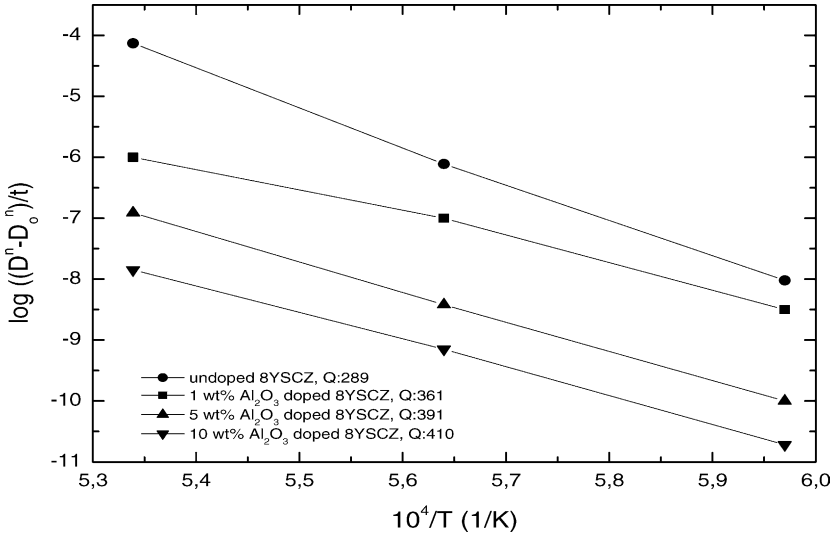

Fig. 6. Arrhenius plots for 8YSCZ containing 0–10 wt.% Al_2O_3.

cations into the matrix, (b) small or no solubility of the solute cations in the matrix, (c) a small interfacial energy between the two phases, (d) a homogeneous distribution of the second phase and (e) stability against dissolution and coarsening.

The grain boundary mobility in pure matter is written as [15]

$$M = \frac{D_{gb}}{\text{б}RT} \quad (4)$$

where D_{gb} is the grain boundary diffusion coefficient, б is the grain boundary width, R is gas constant and T is absolute temperature. As can be seen from this equation, the grain boundary mobility decreases with increasing grain boundary width. Increasing the grain boundary width does not only decrease grain boundary mobility and inhibit grain growth, but also increases the diffusion length over which stress concentration can be rapidly relaxed. Additives and dopants that increase grain boundary width may be effective in minimizing grain growth. However, the mobility is not the only significant influence on grain growth. Grain growth is also dependent on the grain boundary energy. A rate equation for grain growth can be given by [15]

$$D^n - D_o^n = 2M\gamma Vt \quad (5)$$

where D is the instantaneous grain size at time t, D_o is the initial grain size at time $t = 0$, n is the grain growth exponent, M is the mobility, γ is the grain boundary energy and V is the atomic volume. Additives that decrease grain boundary energy have an additional effect on minimizing grain growth. A reduction in grain boundary energy occurs when intergranular phases pin the grain boundaries. The effectiveness of using Al_2O_3 to pin grain boundaries and limit grain growth can be estimated by Zener pinning [16], which describes the dependence of the grain size of matrix on the volume and grain size of second phase as,

$$G = k\left(\frac{r}{f}\right) \quad (6)$$

where G is grain size of matrix, k is constant, r is grain size of second phase and f is volume fraction of second phase. This equation also indicates that grain size of matrix decreases with increasing volume fraction of second phase [16].

In the present study, the differences in grain growth in undoped 8YSCZ and Al_2O_3-doped 8YSCZs can be related to differences in segregation of the solute cations at grain boundaries. SEM with EDS analysis showed that the concentration of Al_2O_3 dopant near the grain boundary region in Al_2O_3-doped 8YSCZ was higher than in undoped 8YSCZ. In the light of the above results, it is deduced that the grain size stability is associated with segregation of solute cation to grain boundaries, which lowers grain boundary mobility and grain boundary energy, thus increasing the cohesive strength of the grain boundary and the diffusion distance across the boundary. Low solubility of Al_2O_3 acts as a barrier against diffusion. Due to the lower solubility of Al_2O_3 in 8YSCZ, grain growth is expected to be slower in Al_2O_3 containing specimens. Compared to Al_2O_3-doped 8YSCZ, undoped 8YSCZ suffers fast grain growth and only limited cation segregation to grain boundaries; consequently, undoped 8YSCZ has a lower grain boundary cohesive strength and a higher grain boundary mobility and energy.

4. Conclusions

The grain growth kinetics and activation energy for grain growth of 8YSCZ having Al_2O_3 additions of 0–10 wt.% were investigated. It was found that the static grain growth exponent value and the activation energy for undoped 8YSCZ were found to be 2 and 289 kJ/mol, respectively. The addition of Al_2O_3 raised the grain growth exponent value to 3 and activation energy for the grain growth process was increased from 289 to 410 kJ/mol for the addition of Al_2O_3 from 0 to 10 wt.%. Grain growth in Al_2O_3-doped 8YSCZ occurs slowly and more sluggishly than that in undoped 8YSCZ. This is mainly due to the lower grain boundary mobility and energy which results from solute segregation in the grain boundary and its drag in Al_2O_3-doped 8YSCZ but not in undoped 8YSCZ. The drag effect arises from any preferred segregation of impurities either to or from grain boundary area because of the size and charge differences. Al_2O_3 addition is expected to segregate to grain boundaries. This segregation layer is believed to hinder grain growth by resulting in limiting matter transfer along the grain boundary.

Acknowledgements

This work has been supported by DPT (the State Planning Organization of Turkey) (under project number 2003K120470-18) and by the Scientific Research Project program of Gazi University (under project number 07/2003-42). The author is grateful to the DPT and Gazi University for their financial support and Kırıkkale University for the provision of laboratory facilities.

References

[1] U. Betz, A. Sturm, J.F. Löffler, W. Wagner, A. Wiedenmann, H. Hahn, Mater. Sci. Eng. A 281 (2000) 68–74.
[2] C.F. Grain, J. Am. Ceram. Soc. 50 (6) (1967) 288.
[3] H.G. Scott, J. Mater. Sci. 10 (9) (1975) 1527.
[4] S.J.T. Kazutaka, Ph.D. thesis, Tokyo University, 2001.
[5] N. Bamba, Y.H. Choa, T. Sekino, K. Niihara, J. Eur. Ceram. Soc. 18 (1998) 693–699.
[6] T. Zhang, Z. Zeng, H. Huang, P. Hing, J. Kilner, Mater. Lett. 57 (2002) 124–129.
[7] I.G. Lee, I.-W. Chen, in: S. Somiya, M. Yoshimura, R. Watanabe (Eds.), Sintering 87, vol. 1, Elsevier, London, 1988, p. 340.
[8] N.-H. Kwon, G.-H. Kim, H.S. Song, H.-L. Lee, Mater. Sci. Eng. A 99 (2001) 185–194.

[9] M.E. Rorabaugh, K.H. Styhr, in: E.M. Lenoe, R.N. Katz, J.J. Burke (Eds.), in: Proceedings of the Conference of the Army Materials Technology, Washington, 1979, pp. 309–322.
[10] A.J. Burggraaf, A.J. Winnubst, in: J. Nowotny, L.C. Dufour (Eds.), Surface and Near-Surface Chemistry of Oxide Materials, Elsevier, Amsterdam, 1988, pp. 449–474.
[11] M. Mori, M. Yoshikawa, H. Itoh, T. Abe, J. Am. Ceram. Soc. 8 (1994) 2217–2219.
[12] J. Zhao, Y. Ikuhara, T. Sakuma, J. Am. Ceram. Soc. 81 (8) (1998) 2087–2092.
[13] I.W. Chen, L.A. Xue, J. Am. Ceram. Soc. 73 (1990) 2585.
[14] A. Sturm, U. Betz, U. Scipione, H. Hahn, NanoStruct. Mater. 11 (5) (1999) 651–661.
[15] D. Turnbull, Trans. AIME 191 (1951) 78.
[16] A.A. Sharif, P.H. Imamura, M.L. Mecartney, Mater. Sci. Forum 304–306 (1999) 443–450.